

Received: 2016.04.27  
Accepted: 2016.05.30  
Published: 2016.07.21

# Effect of Different Rotational Directions of BJUT-II VAD on Aortic Swirling Flow Characteristics: A Primary Computational Fluid Dynamics Study

Authors' Contribution:  
Study Design A  
Data Collection B  
Statistical Analysis C  
Data Interpretation D  
Manuscript Preparation E  
Literature Search F  
Funds Collection G

A **Qi Zhang**  
CD **Bin Gao**  
BCDG **Yu Chang**

School of Life Science and BioEngineering, Beijing University of Technology, Beijing, P.R. China

**Corresponding Author:** Yu Chang, e-mail: changyu@bjut.edu.cn

**Source of support:** This work partly was sponsored by the National Natural Science Foundation of China (Grant No. 11072012, 10872013, 31070754). This work was also sponsored by the Beijing Municipal Education Commission Foundation (Grant No. KM201510005028), BJUT Talent Found (Grant No.2014000020124G045), and BJUT Foundation Fund (Grant No. 015000514316007)

**Background:** The BJUT-II VAD is a novel left ventricular assist device (LVAD), which is thought to have significant effects on the characteristics of aortic swirling flow. However, the precise mechanism of the rotational direction of BJUT-II VAD in the aortic swirling flow is unclear.

**Material/Methods:** A patient-specific aortic geometric model was reconstructed based on the CT data. Three pump's output flow profiles with varied rotational direction, termed "counterclockwise", "flat profile", and "clockwise", were used as the boundary conditions. The helicity density, area-weighted average of helicity density (Ha), localized normalized helicity (LNH), wall shear stress (WSS), and WSS spatial gradient (WSSG) were calculated to evaluate the swirling flow characteristics in the aorta.

**Results:** The results demonstrated that the swirling flow characteristics in the aorta and 3 branches are directly affected by the output blood flow of BJUT-II VAD. In the aortic arch, the helicity density, supported by the clockwise case, achieved the highest value. In the 3 branches, the flat profile case achieved the highest helicity density, whereas the maximum WSS and WSSG generated by clockwise case were lower than in other cases.

**Conclusions:** The outflow of the BJUT-II VAD has significant effects on the aortic hemodynamics and swirling flow characteristics. The helical blood profiles can enhance the strength of aortic swirling flow, and reduce the areas of low WSS and WSSG regions. The clockwise case may have a benefit for preventing development of atherosclerosis in the aorta.

**MeSH Keywords:** **Aorta • Heart-Assist Devices • Hemodynamics**

**Full-text PDF:** <http://www.medscimonit.com/abstract/index/idArt/899313>

 4313  1  9  47



## Background

Heart failure is a severe cardiovascular disease. Left ventricular assist devices (LVADs) have become a very important treatment method for heart failure [1]. Along with the increased clinical use of LVADs, the hemodynamic effects of LVADs on the cardiovascular system have been attracting research interest. For instance, Karmonik et al. [2] studied the influence of LVAD cannula outflow tract location on hemodynamics in the ascending aorta, reporting that variation in the position of the cannula outflow clearly affected hemodynamics in the ascending aorta, favoring an anterior geometry for a more ordered flow pattern. Subsequently, Song et al. [3] researched the hemodynamic effects of various support modes of continuous flow LVADs on the cardiovascular system, and demonstrated that the continuous flow control mode of the CF-LVAD achieves the highest ventricular unloading. Most recently, Karmonik et al. [4] compared the hemodynamics in the ascending aorta in pulsatile vs. continuous flow left ventricular assist devices, and found superior performance of pulsatile LVADs. In addition, Osorio et al. [5] demonstrated that the LVAD implantation geometry was an important factor regulating hemodynamic states in the aorta.

The swirling flow in the blood vessels is an important research area of hemodynamics. In recent years, the swirling flow in the aorta has aroused wide concern. Bogren et al. [6] found that people of different ages have swirling flow in the aorta. Similarly, Deng [7] reported on swirling flow in human aortic vascular blood flow. This kind of flow pattern is desirable for blood flow stability and reduced turbulence, and to smooth blood vessel walls by scouring and reducing harmful substances in vessel wall deposits. In addition, Stonebridge [8] found that swirling flow can more efficiently transport blood. Similarly,

Deng's [9] studies shown that improving swirling flow intensity can significantly increase the aortic wall shear stress and reduce the scope of the intraaortic blood flow stagnation zone. Qiu et al. [10] reported that increased swirling flow strength could inhibit vascular endothelial cell proliferation and smooth muscle cell apoptosis. In short, the above-mentioned studies confirmed that swirling flow plays an important role of maintaining normal aortic structure and function. However, there is has been no study published on the effects of LVADs on the characteristics of aortic swirling flow.

BJUT-II VAD (previously called an intra-aorta pump) is a novel LVAD [11], which is implanted into the ascending aorta (Figure 1), and the blood is directly pumped through the aortic valve into the aorta. Few studies on the hemodynamic effects of BJUT-II VAD on the cardiovascular system have been conducted. Gao [12] proposed a pulsatile control strategy to provide adequate perfusion and restore the blood pulsatility. After that, the blood assist index (BAI) was proposed to quantify the unloading level and to evaluate the hemodynamic states of the left ventricle [13–16]. Subsequently, the hemodynamic effect of varied support modes of BJUT-II VAD on the cardiovascular system has been studied. In contrast to conventional LVADs, under co-pulse mode the BJUT-II VAD can achieve maximum left ventricular unloading and coronary perfusion and can restore the blood pulsatility [17–19]. Most recently, the hemodynamic effects of the BJUT-II VAD on the aorta has been investigated by using computational fluid dynamics (CFD) method [20]. The results demonstrated that the hemodynamic effect of BJUT-II VAD is quite different from that caused by conventional LVADs [21].

Although the effects of LVADs on aortic hemodynamics have been studied, the effects of the helicity components of LVADs'

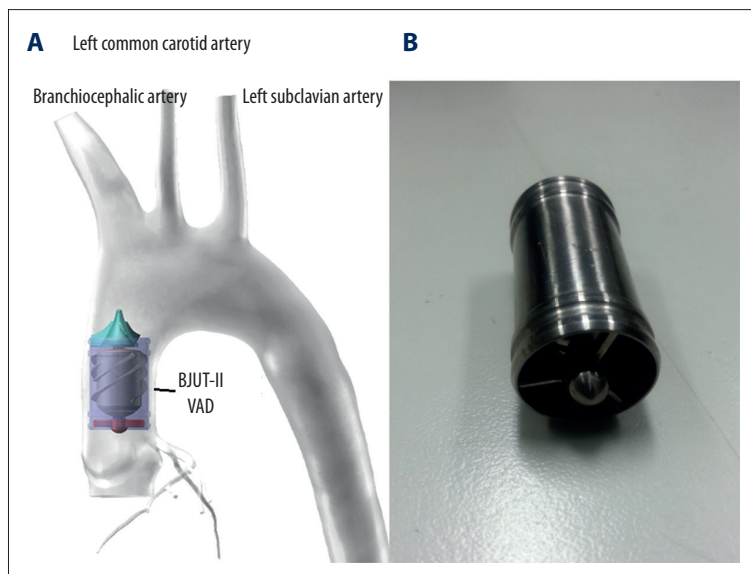


**Figure 1.** (A) Implanted position of BJUT-II VAD. (B) Actual photos of BJUT-II VAD.

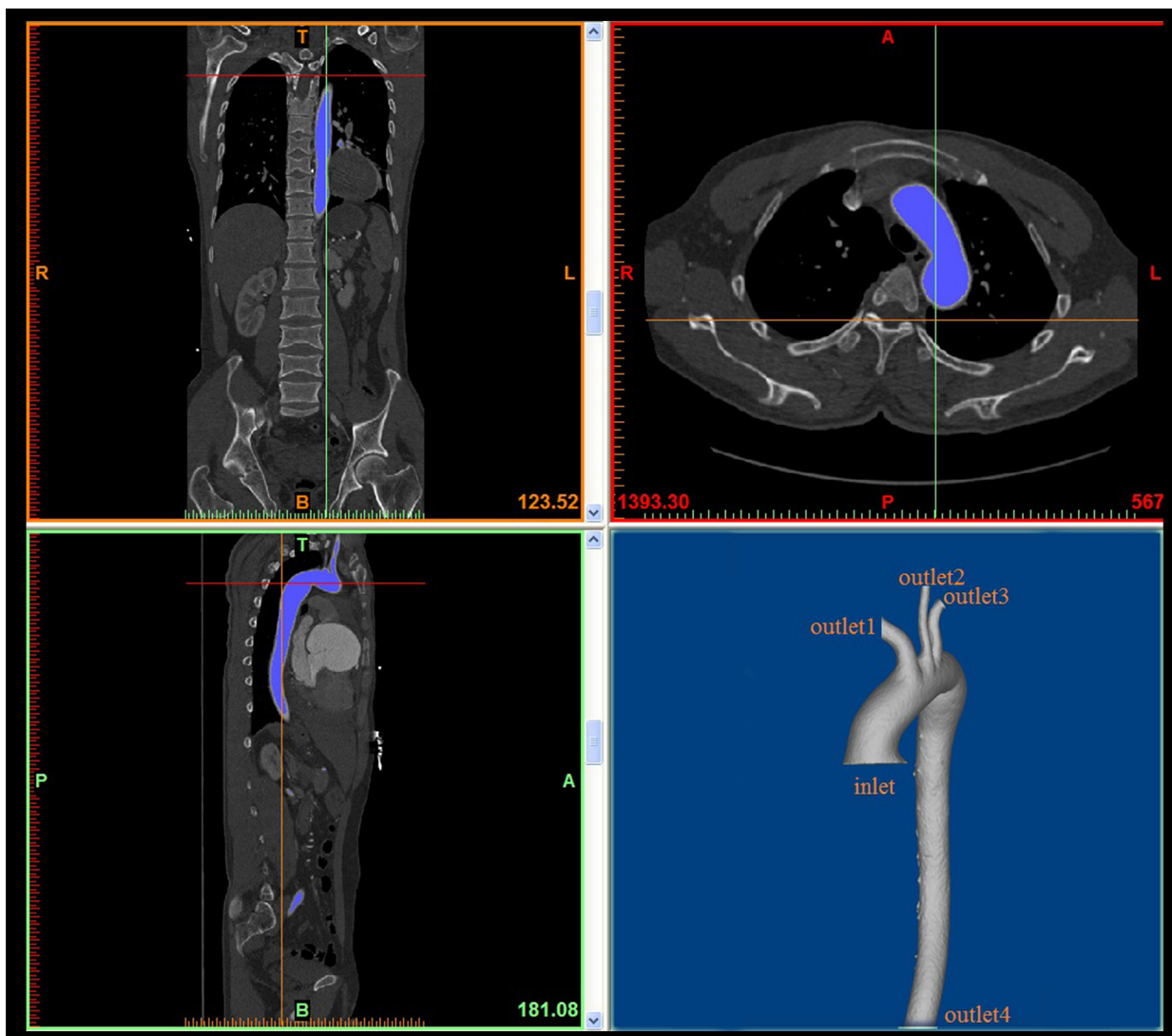


**Figure 2.** Geometric model of patient-specific aorta constructed from CT data.

outflow on the aorta are still ignored by researchers, as the helical component is considered to be too low to change the aortic hemodynamic states under conventional LVAD support. Because the BJUT-II VAD is directly implanted into the aorta, the effects of helicity components in its outflow on the aorta cannot be ignored. However, its precise effects are still unclear.

In this work, we performed numerical simulations to clarify the effects of varied rotational direction of BJUT-II VAD on the aortic swirling flow characteristic. A patient-specific aortic geometric model was reconstructed based on CT data. Three cases of outflow of BJUT-II VAD, termed “counterclockwise case”, “flat profile case” and “clockwise case”, were used in this study as the boundary conditions. The helicity density, area-weighted average of helicity density (Ha), localized normalized helicity (LNH), wall shear stress (WSS), and WSS spatial gradient (WSSG) were calculated to quantitate swirling flow characteristics in the aorta.

## Material and Methods

### Aortic model reconstruction

The aortic model was reconstructed by using MIMICS15.0 (MATERIALISE, Belgium) based on the CTA data from a heart failure patient. The resolution of CTA data was 512×512, the pixel size was 0.91 mm, and the layer spacing was 1 mm. The aortic model (Figure 2) consisted of the ascending aorta, the brachiocephalic artery, the left common carotid artery, the left subclavian artery, and the descending aorta. The ANSYS ICEM 14.5 (ANSYS, Inc., USA) was used to generate the non-structural tetrahedral meshes for the model (Figure 3). A grid independence test was conducted to determine the optimal grid numbers for the computation. In this test, the flow velocity is chosen as the inlet boundary condition, while pressure waveform is set as the outlet boundary condition. The relative

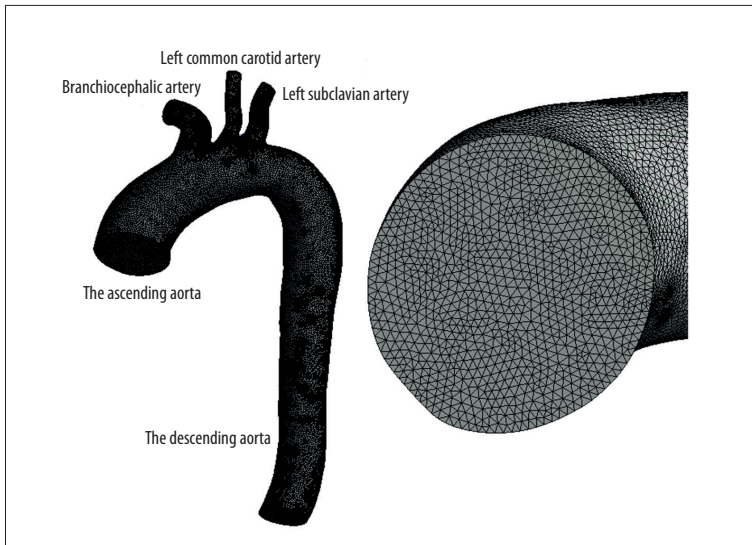


**Figure 3.** Geometry and mesh for models of thoracic aorta.

**Table 1.** Grid independence test.

Nodes	Elements	Pressure (Pa)	Relative error (%)
42364	225334	1588.36	4.09%
80264	438641	1653.31	4.76%
153530	855132	1732.05	3.46%
307813	1701015	1792.02	2.25%
367909	2089916	1746.26	

errors of pressure at the inlet of the model with the different numbers of elements are calculated. If the relative error is less than 3%, the number of elements is considered to be adequate. The test results are listed in Table 1. According to the results, 1.72 million elements were sufficient for this study.

### Numerical approaches

#### Governing equations

The blood flow of aorta calculation is based on 3-dimensional incompressible Navier-Stokes equation (1) and (2):

$$\rho(\vec{u} \cdot \nabla) \vec{u} = -\nabla p + \mu \Delta \vec{u} \quad (1)$$

$$\nabla \cdot \vec{u} = 0 \quad (2)$$

where  $\rho$  stands for the density of blood flow,  $\vec{u}$  is the fluid velocity vector,  $p$  represents the pressure, and  $\mu$  denotes the dynamic viscosity.

#### Boundary conditions

In order to protect the function of aortic valve, the aortic valve was opened periodically throughout the simulation. The

time-varying boundary conditions were taken from a previously validated lumped parameter model of assisted cardiovascular system [22,23] and applied directly as the flow rate and pressure at the inlet and outlet of the model, respectively. The mathematic model of the cardiovascular-pump system was used in the LVAD control algorithm test. Figure 4 shows the complete electric circuit analogy of the cardiovascular model in relation to the LVAD. The model comprises left atria, active left ventricular, intra-aorta pump, and peripheral circulation system.

To investigate the effect of different rotational directions of BJUT-II VAD on the aortic swirling flow characteristics, 3 outflow profiles of BJUT-II VAD with varied rotational direction were obtained as the inlet flow profiles (Figure 4). Among them, the counterclockwise case and clockwise case were taken from a validated CFD simulation of the BJUT-II VAD, operated at a constant impeller speed of 8000 rpm with counterclockwise rotational direction and clockwise rotational direction, respectively. Outflow profiles differ from the flat profile in the rotational component of the outflow profiles, which is a result of the rotating impeller. The velocity profile was scaled to follow the time-varying inlet flow rate of the 0D model to allow comparisons to be made against simulations with a flat inlet profile.

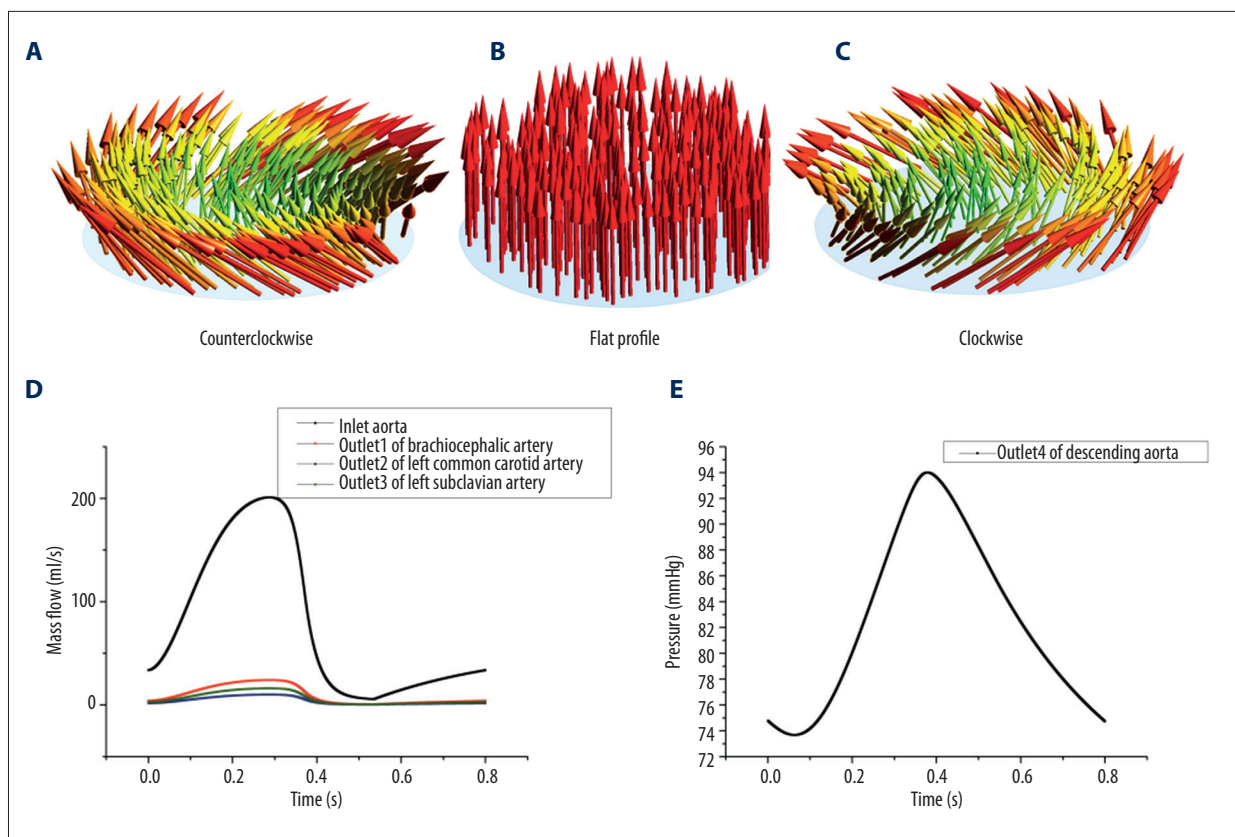


**Figure 4.** The boundary conditions in this study. (A) Is the inlet blood flow with counterclockwise direction; (B) Is the flat profiles of the inlet blood flow; (C) Is the blood flow with clockwise direction; (D) Is the blood flow boundary condition; (E) Is the pressure outlet boundary condition.

The 3 cases shown in Figure 4, termed “counterclockwise”, “flat profile”, and “clockwise”, were used in this study as the boundary conditions of the inlet of the aortic model. The first case is counterclockwise case, in which the blood flow is consistent with the left hand rule (Figure 4A). This case represents the outflow condition of BJUT-II VAD when BJUT-II VAD is operated under counterclockwise direction. The second case is flat profile case, which does not include the helical components (Figure 4B). This case was used as the control group to evaluate the hemodynamic effect on the aorta, when the helical component of the outflow is ignored. The last case is the clockwise case, in which the blood flow was in line with the right hand rule (Figure 4C). This case denotes the outflow condition of BJUT-II VAD when it runs under clockwise direction.

**Computation settings**

In this study, the vessel wall is assumed to be no-slip condition, and the blood is treated as a homogeneous, incompressible Newtonian fluid with a constant density and viscosity ( $\rho=1050\text{kg/m}^3$ ,  $\mu=0.0035\text{pa s}$ ). The numerical simulations were carried out by using Fluent (Ansys. Inc., USA). Each time step was taken to be numerically converged once the root

mean-squared residuals of pressure and momentum, in all 3 directions, reached a value below  $10^{-6}$ . According to the geometric size of the aorta, the peak systolic blood flow velocity, and the blood density, the peak systolic Reynolds number  $Re$  is larger than 5000. Hence, the k-e turbulence model, proven to be appropriate for illustrating the turbulence flow states in the aorta [24], was used in this study. The simulations employ a time step of 1 ms and were run for 4 cardiac cycles to remove any initialization effects. The hemodynamic parameters in the fourth cardiac cycle were extracted for hemodynamic analysis.

**Hemodynamics analysis**

Helicity density is an important indicator for quantifying swirling flow [25], which is represented as the scalar product of velocity and vorticity in the field, defined as equation (3):

$$H_d = \vec{V}(\nabla \times \vec{V}) \quad (3)$$

where  $\vec{V}$  is the velocity vector. Vorticity is a measure of the rotation of a fluid element as it moves in the flow field, and is defined as the curl of the velocity vector ( $\nabla \times \vec{V}$ ).

In this study, a helicity density indicator was used to evaluate the strength of swirling flow; hence, equation (3) was simplified to equation (4):

$$H = |H_d| = |\vec{V}(\nabla \times \vec{V})| \quad (4)$$

It was proved that the rotating direction of blood flow, defined as the angle between the velocity vector and the vorticity vector, is closely related to the occurrence of vascular disease [26]. The localized normalized helicity (LNH) [27] was proposed to evaluate this characteristic, shown as equation (5):

$$LNH(s; t) = \frac{V(s; t) \cdot \omega(s; t)}{|V(s; t)| |\omega(s; t)|}, -1 \leq LNH \leq 1 \quad (5)$$

where  $\vec{v}$  is the velocity vector,  $\omega$  is the vorticity vector,  $s$  is the position, and  $t$  denote the time instant. The LNH value ranges from  $-1$  to  $+1$ .  $-1$  means that the left-handed helicity component of blood flow (aortic swirling flow is clockwise rotation) is dominant, while  $+1$  denotes that the right-handed helical components of the blood flow (aortic swirling flow is clockwise rotation) is dominant.

In order to characterize the strength of swirling flow in the aorta better, the area-weighted average of helicity density (Ha) [25] was calculated as the equation (6):

$$H_a = \frac{1}{S} \int H_d dS \quad (6)$$

where  $S$  is the cross-sectional area and  $H_d$  represents the helicity density; it can effectively describe the strength of swirling flow in the aorta.

### Wall shear stress (WSS)

Stress is calculated as a function of time during the cycle at each location using least-squares fit of 3 radial stations measured very close to the wall according to the defining relationship [28], as the equation (7):

$$\vec{\tau}_\omega = \mu \frac{\Delta \vec{v}}{\Delta r} \quad (7)$$

where  $\vec{\tau}_\omega$  is the wall shear stress,  $\mu$  is the absolute viscosity,  $\vec{v}$  is the velocity parallel to the wall, and the  $r$  is the radial distance from the wall.

### WSS Spatial Gradient (WSSG)

The wall shear stress spatial gradient is given by [26], shown as the equation (8):

$$WSSG = \frac{1}{T} \int_0^T \sqrt{\left(\frac{\partial WSS_x}{\partial x}\right)^2 + \left(\frac{\partial WSS_y}{\partial y}\right)^2 + \left(\frac{\partial WSS_z}{\partial z}\right)^2} dt \quad (8)$$

where  $x, y, z$  are the 3 directions of the global coordinate system.

## Results

### The distribution of helical density in the aorta

Figure 5 shows the distribution of helical density in the aorta under varied cases. In order to compare the results, the helicity density generated by varied cases at the 4 specific time points (from T1 to T4) was selected. At T1, obvious swirling flow under counterclockwise and clockwise cases exists in region A. However, no swirling flow was observed under flat profile case. The helicity density at region A generated by 3 cases was  $4.56 \text{ m/s}^2$ ,  $2.14 \text{ m/s}^2$ , and  $6.57 \text{ m/s}^2$ , respectively. Similarly, the helicity density at region A has been strengthened under the counterclockwise case and clockwise case (counterclockwise:  $6.98 \text{ m/s}^2$ , clockwise:  $6.77 \text{ m/s}^2$ ) at T2. Moreover, there was a high helicity density value region under clockwise case (clockwise:  $11.37 \text{ m/s}^2$ ) in region C. In region D, 3 bifurcation helicity density was significantly higher in the flat profile case than in the other 2 assisted cases (counterclockwise:  $11.56 \text{ m/s}^2$ , flat profile:  $18.79 \text{ m/s}^2$ , and clockwise:  $7.86 \text{ m/s}^2$ ). At time point T3, under the counterclockwise and clockwise case, region B showed very strong swirling flow, but there was a vortex under the flat profile case. In the 3 cases, region C helicity density was far greater than in other regions (region C, counterclockwise:  $9.87 \text{ m/s}^2$ , flat profile:  $9.06 \text{ m/s}^2$ , clockwise:  $10.03 \text{ m/s}^2$ ). At time T4, the helicity density was low under varied cases.

### The distribution of LNH in the aorta

Figure 6 shows the distribution of LNH under varied cases. The blood flow under counterclockwise case contains many counterclockwise swirling flow components in the aorta. However, under both the flat case and clockwise case, the blood flow involves many clockwise swirling flow components in the aorta. The area of clockwise swirling flow under clockwise case was larger than clockwise swirling flow under flat profile case. In addition, the blood flow in the ascending aorta appears to have a clockwise rotation swirling flow under counterclockwise case at the time point T3.

### Area-weighted average of helicity density (Ha)

Figure 7 illustrates change in the area-weighted average of helicity density (Ha) of 8 representative slices (from S1 to S8) along the aortic model under different cases. For all cases, the Ha was gradually increased along with the axis of the aorta, and then it achieves its maximum value at S5. After that, Ha is gradually decreased along with the axis of the aorta. Moreover, Ha under both clockwise case and counterclockwise case was larger than that under flat profile case. The averaged Ha value under clockwise case was higher than in counterclockwise case (counterclockwise:  $5.69 \text{ m/s}^2$ , flat profile:  $3.91 \text{ m/s}^2$ , clockwise:  $5.75 \text{ m/s}^2$ ).

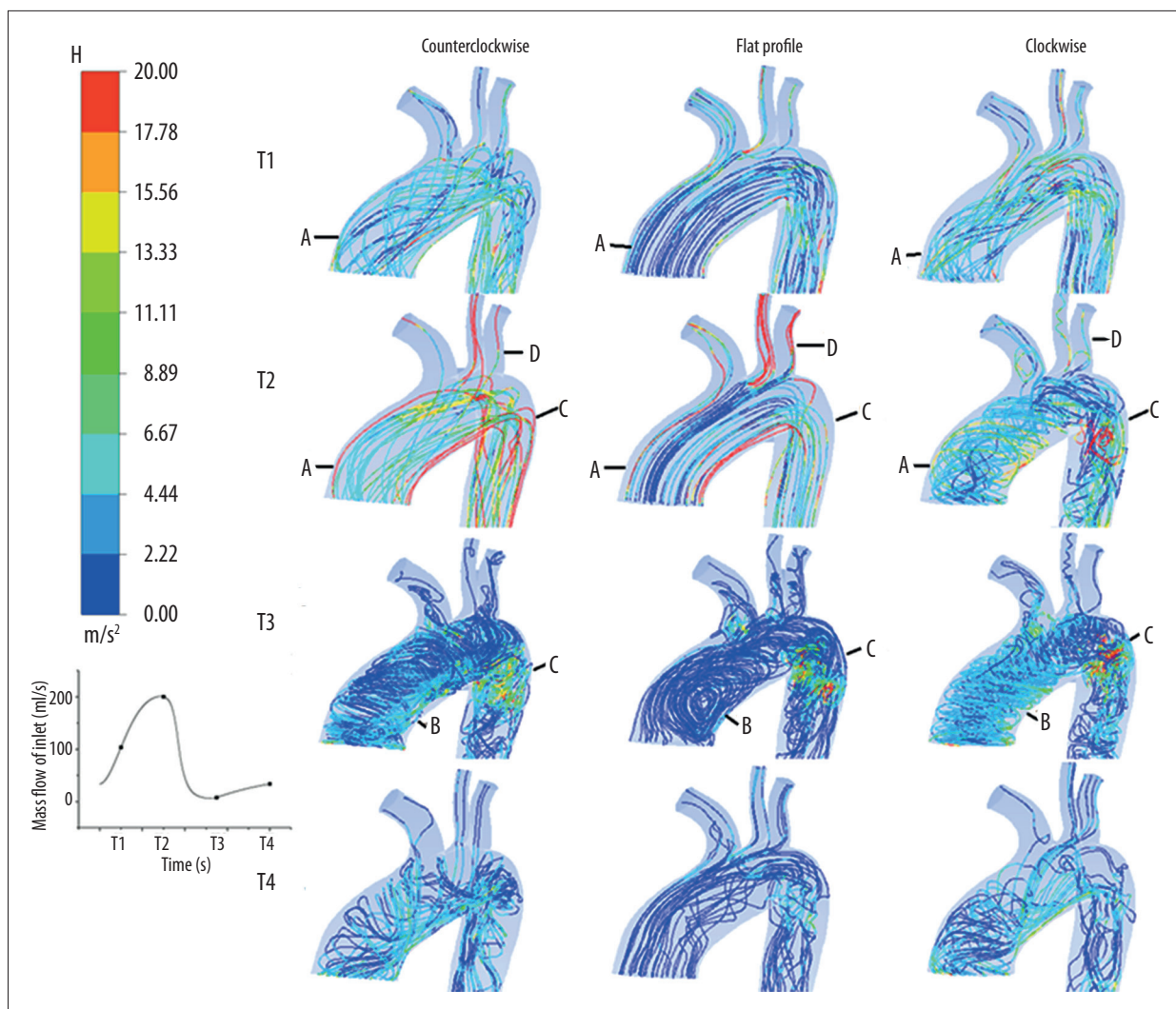


**Figure 5.** Pathlines of helical density in the aorta under varied cases. In the figure, the magnitude of helical density was coded by color, and the color bar in the left of the figure shows the color scale with units of meter per second squared. The pathlines of helical density occurring at 4 times are shown in the figure. The left bottom figure in Figure 5 shows the selected diagram of inlet mass flow-specific time.

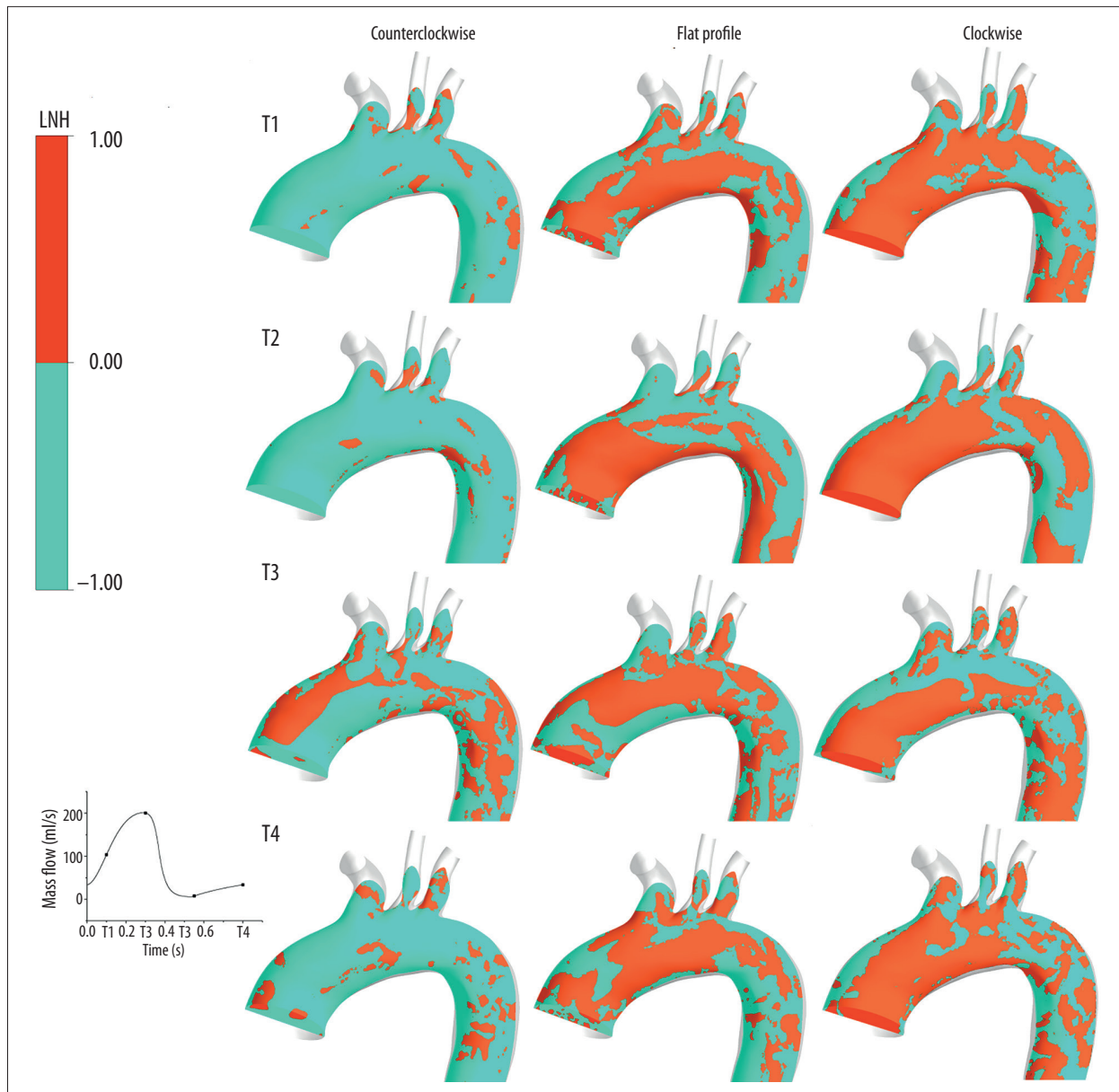
**The distribution of WSS in the aorta**

Figure 8 illustrates the distributions of WSS under 3 cases. WSS under counterclockwise cases ranged from 0 Pa to 50.48 Pa, the WSS under flat profile case ranged from 0 Pa to 25.26 Pa, and WSS under clockwise case ranged from 0 Pa to 8.8 Pa. At the time point T1, the WSS value was larger assisted by clockwise case than other cases at region A (counterclockwise: 1.98 Pa, flat profile: 1.58 Pa, clockwise: 2.36 Pa). Similar, the WSS generated by counterclockwise case was lower than flat profile case at region B (counterclockwise: 0.87 Pa, flat profile: 1.33 Pa). However, the WSS assisted by clockwise case was higher than flat profile case (flat profile: 1.33 Pa, clockwise: 1.53 Pa). At time point T2, the WSS achieved its maximum at region C under all cases (counterclockwise: 7.56 Pa, flat profile:

7.73 Pa, clockwise: 7.66 Pa). Moreover, the WSS in region D was significantly lower than in other areas. In region D, the WSS generated by clockwise case was larger than other cases at time point T3. (counterclockwise: 0.57 Pa, flat profile: 0.64 Pa, clockwise: 1.88 Pa). At the time point T4, in most areas, WSS was very low, while WSS under clockwise case at region A was significantly higher than that under other cases (counterclockwise: 1.86 Pa, flat profile: 0.55 Pa, clockwise: 2.25 Pa).

**The distribution of WSSG at aorta**

Figure 9 shows the distribution of WSSG under varied cases. The WSSG, generated by counterclockwise case, ranged from 0 to 33,404 Pa/m. The WSSG, caused by flat profile case, ranged from 0 to 36,843 Pa/m. And the WSSG, under clockwise cases,



**Figure 6.** The distribution of LNH under varied cases. Figure 7 consists of 3 parts: a unified scale for LNH under varied cases; the selected diagram of inlet mass flow-specific time; and the most important part is the contour plot of LNH in the aorta under varied cases.

ranged from 0 to 28,525 Pa/m. At time point T1, the WSSG value at region A assisted by flat profile case was lower than that assisted by other cases (counterclockwise: 324.32 Pa/m, flat profile: 175.89 Pa/m, clockwise: 358.64 Pa/m). For all cases, the large level WSSG value was found at region A (counterclockwise: 453.25 Pa/m, flat profile: 462.33 Pa/m, clockwise: 471.63 Pa/m). At the time point T2, the WSSG value generated by clockwise case was larger than other cases (counterclockwise: 189.22 Pa/m, flat profile: 193.54 Pa/m, clockwise: 376.28 Pa/m). For all cases, the WSSG achieved its maximum at region D (counterclockwise: 1809.37 Pa/m, flat profile: 1874.65 Pa/m, clockwise:

1376.63 Pa/m). At time point T3 and T4, the WSSG assisted by 3 cases was very low. At the time point T3, the WSSG generated by clockwise case was larger than other cases (counterclockwise: 408.29 Pa/m, flat profile: 157.67 Pa/m, clockwise: 421.55 Pa/m).

## Discussion

Although there are many studies on the hemodynamic effect of LVAD on the aorta, all of them focus on the change in the pressure and perfusion level of LVAD. The present study is the

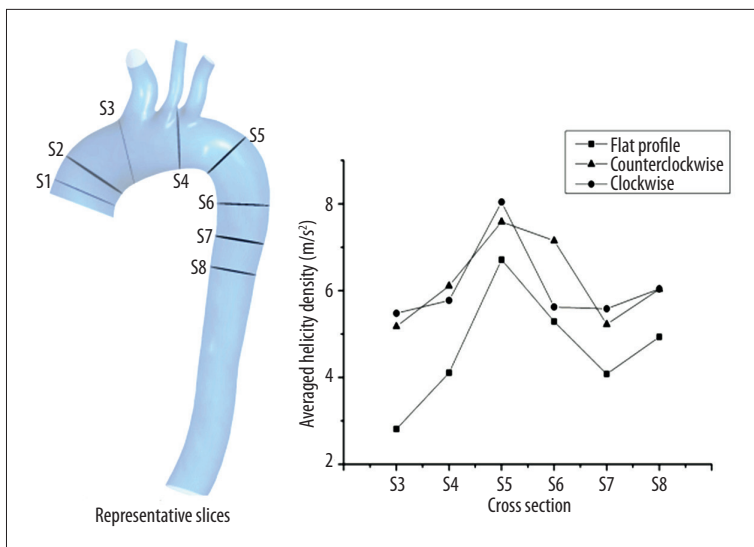


**Figure 7.** Plots of area-weighted average of helicity density at 8 representative slices under 3 cases.

first on the effect of the rotational direction of outflow on the swirling flow characteristics in the aorta. The results demonstrate that the rotational direction of the pump’s outflow has significant effects on the hemodynamic states and the swirling flow characteristic in the aorta.

Although use of LVADs have been confirmed as a useful alternative treatment for heart failure patients, the increase in related complications caused by LVAD support raised widespread concerns. For instance, Ambardekar et al. reported that the aortic wall stiffness was significantly increased with the use of LVAD support [29]. Similarly, Templeton et al. reported that vascular compliance was impaired by the use of LVAD support [30]. In addition, Hasin et al. found that the peripheral endothelial function was attenuated after LVAD therapy [31]. From the hemodynamic view point, the changes in hemodynamic states, especially in the swirling flow characteristic, play an important role in these complications. The present study demonstrates that the rotational direction of BJUT-II VAD can directly change the hemodynamic states and swirling flow characteristic. Therefore, the incidence of complications caused by LVAD may be reduced by choosing an appropriate rotational direction of LVAD. Moreover, our study also shows that the structure of LVADs should be designed not only for satisfactory hydraulic properties, but also for optimal blood flow pattern in the aorta.

Helicity density is an important indicator for quantifying the swirling flow in the aorta, which can effectively describe helicity intensity of aortic flow. Houston et al. [32] found that the aortic arch in the presence of swirling flow is associated with the increase of carotid atherosclerotic plaque. Yashiro et al. [33] found that geometric structure is one of the causes of aortic swirling flow. Javadzadegan et al. [34] found that an increase in the intensity of spiral flow resulted in an increase

in maximum wall shear stress (WSS) and a decrease in maximum wall stress, thereby reducing the risk of rupture, endothelial dysfunction, and the development of atherosclerosis. Fan et al. [35] reported that the swirl flow can significantly reduce the aorta area within the low wall shear stress, and, as the decrease of intensity of swirling flow, aortic blood flow low velocity area is significantly increased. In our study, the helicity density of blood flow under clockwise case was significantly larger than in the other 2 cases (Figure 5). This means that an LVAD generating clockwise outflow may help prevent endothelial dysfunction and thrombi generation. In the future, the rotational direction of the impeller should receive more attention to generate the optimal swirling flow level.

LNH is also an important indicator of quantification swirling flow in the aorta, and is a useful descriptor of changes in the direction of the rotation of flow because a change in sign of the local value of LNH can identify a local right/left-handed rotation. Chien [36] found that changes in the direction of blood flow have effects on the magnitude and direction of WSS, thereby affecting the vascular structure and function. ECs can influence vascular remodeling, modulate thrombosis, mediate inflammatory responses, and regulate vascular smooth muscle cell contraction. As shown in Figure 6, the results show that the different support directions of BJUT-II VAD significantly affect the swirling flow in the aorta and its 3 branches. This means the rotational direction of BJTU-II VAD may have significant effects on endothelial function, which may be one of the reasons for the vascular complications caused by LVAD support.

Figure 7 shows that the helicity density of swirling flows is significantly enhanced under clockwise and counterclockwise cases. Gallo et al. [37] demonstrated that high helicity intensity was instrumental in suppressing flow disturbances; this protective effect could be moderated when a direction of rotation was

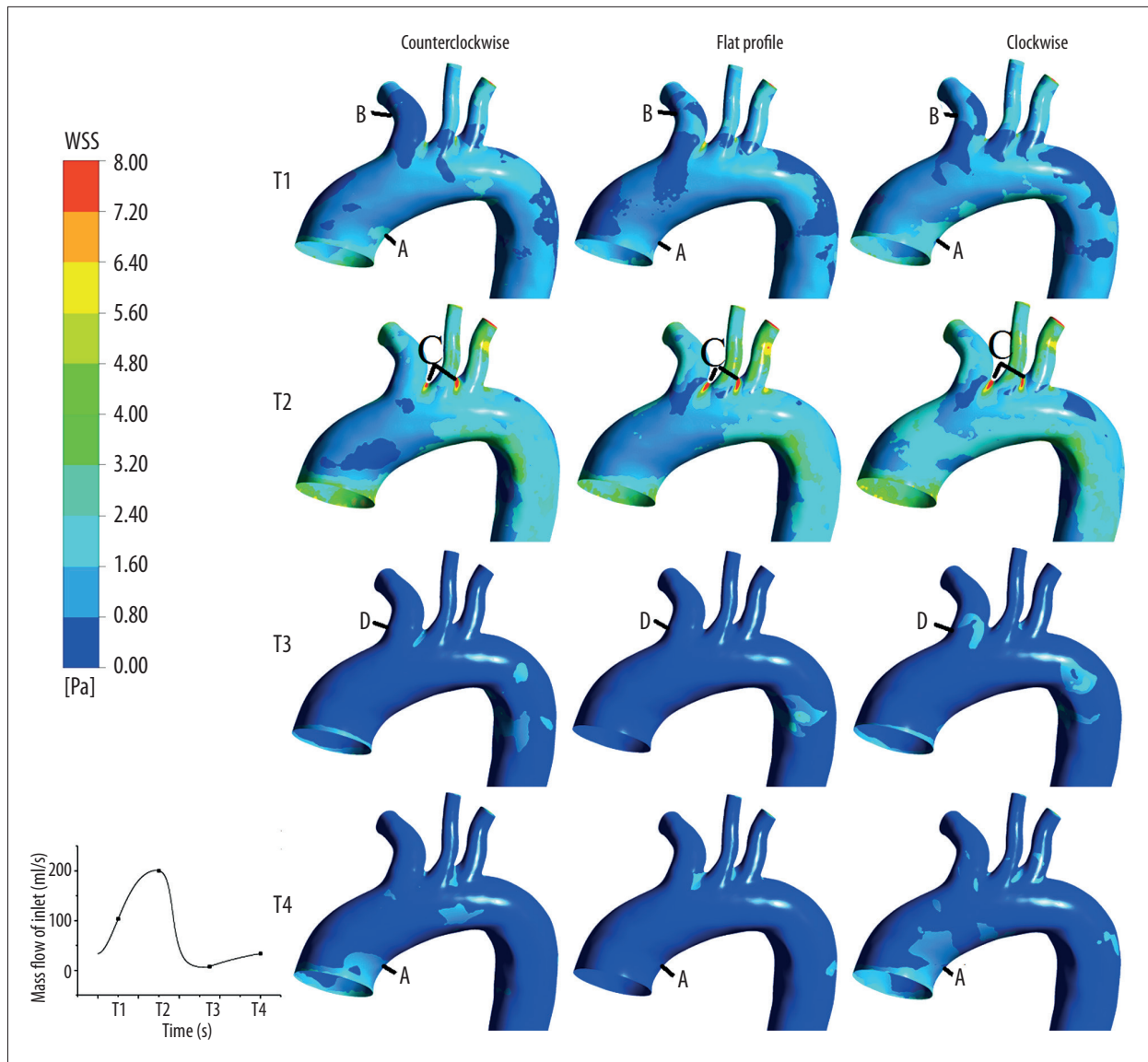


**Figure 8.** Comparison of WSS under different cases. In the figure, the magnitude of WSS was coded by color, and the color bar in the left of the figure shows the color scale with units of Pa. The WSS occurring at 4 specific times are shown in Figure 9. The left bottom figure in Figure 8 shows the selected diagram of inlet mass flow characteristic time.

dominant in the flow field. Morbiducci et al. [38] confirmed that helical flow constituted an important flow signature in vessels, and its strength is a fluid dynamic index for risk stratification, in the activation of both mechanical and biological pathways leading to fibrointimal hyperplasia. Paul et al. [39] showed that the spiral effect of swirling flow could reduce turbulent kinetic energy, which is a beneficial effect.

The local wall shear stress can be used as an indicator of disturbed flow, which identifies the regions where a potential arterial disease process may start [40]. As shown in Figure 8, at time point T1, the WSS value in the aortic arch (at region A) assisted by flat profile case was lower than in other cases.

The result shows that the WSS value in the aortic arch was improved by the output blood flow of BJUT-II VAD with rotational directions. Jennifer [41] pointed out that low WSS had strong relevance to atherogenesis. Hence, the counterclockwise case and clockwise case may have a benefit for preventing atherosclerosis in the aortic arch. However, the left common carotid under counterclockwise case is more likely to form atherosclerosis. In all cases, the WSS at region D was very low at time point T2. Bakey et al. [42] found some special positions of blood vessels, such as curvatures, bifurcations, tortuosity, and branching, where shear stress is reduced. Experimental results *in vivo* have shown that low WSS can cause intimal wall thickening [43] and lead to thrombi generation [21]. At time

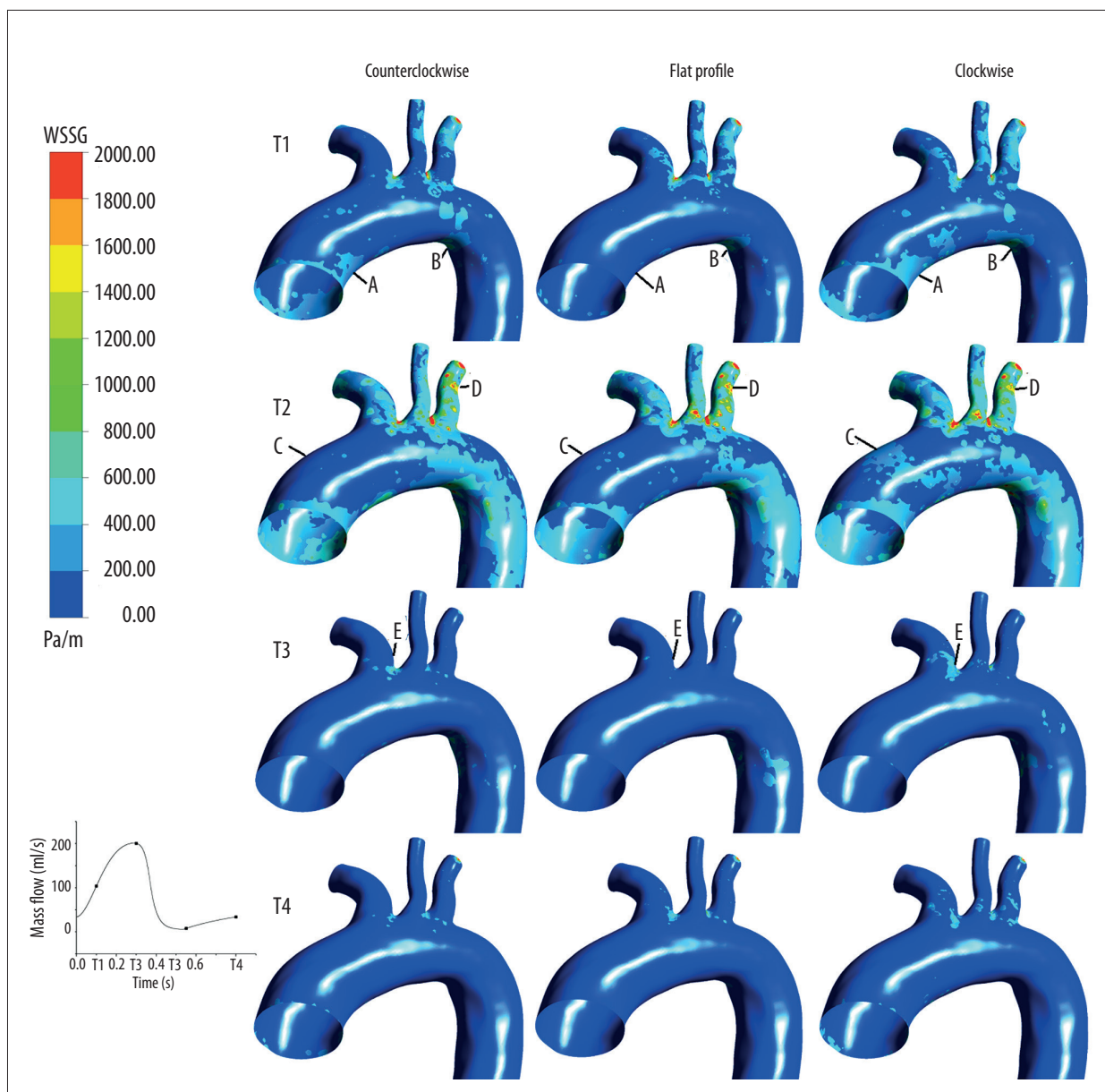


**Figure 9.** Distribution of WSSG under varied cases. In the figure, the magnitude of WSSG was coded by color, and the color bar in the left of the figure shows the color scale with Palmer units per meter. The WSSG occurring at 4 times are shown in the Figure. The left bottom figure in Figure 9 shows the selected diagram of inlet mass flow-specific time.

point T2, the WSS values at region C exceed 7 Pa. Malek [44] found that over 1 cardiac cycle, instantaneous WSS magnitude typically ranges from 1 to 7 Pa in the arterial system. Jennifer [41] found that high WSS is associated with outward remodeling of vessels. At time point 3, the WSS value in the left common carotid roots generated by clockwise case was higher than in other cases

Depaola et al. [45] speculated that large shear stress gradients could induce morphological and functional changes in the endothelium in regions of disturbed flow *in vivo* and thus

may contribute to the formation of atherosclerotic lesions. Lei et al. [46] suggested that the local wall shear stress gradient (WSSG) was the single best indicator of nonuniform flow fields leading to atherogenesis. Jeffrey et al. [47] found that large spatial shear stress gradients had anecdotally been associated with early atherosclerotic lesion susceptibility *in vivo* and have been proposed as promoters of endothelial cell dysfunction *in vitro*. In this study, the maximum WSSG value generated by flat profile was higher than in other cases. Hence, atherosclerosis may more easily form under flat profile than in the other 2 cases.

The research results show that the rotation direction of the pump can directly affect the distribution of swirling flow inside the blood vessels, thereby affecting vascular cell growth and deposition of various macromolecules. Therefore, the results of our study suggest that when we design an LVAD in the future, in addition to focusing on the indicators of output flow and pressure, the direction of rotation and output flow field of swirl flow characteristics also should be considered and optimized. In addition, the physiological effects of this swirling flow caused by pump rotation direction require further clarification by biomechanical studies. The present study only investigated the effect of the swirling flow field of different rotation directions on aortic flow field. In practical application, changing the pump structure can change the swirl intensity of output flow. This change will cause intravascular hemodynamic significant variations, which needs further study.

## Conclusions

A numerical study was conducted to investigate the hemodynamic effects of different rotational directions of BJUT-II VAD on aortic swirling flow characteristics. A patient-specific aortic geometric model was reconstructed based on CT data. We used 3 cases of pump output flow field with varied rotational directions, termed “counterclockwise”, “flat profile”, and “clockwise”, as the boundary conditions of the inlet of the aortic model. The results demonstrate that the swirling flow characteristics in the aorta and its 3 branches are directly affected by the output blood flow in the BJUT-II VAD with varied

rotational directions. In the aortic arch, the helicity density, supported by the clockwise case, achieved the highest value among the 3 cases (region c, counterclockwise:  $9.87 \text{ m/s}^2$ , flat profile:  $9.06 \text{ m/s}^2$ , clockwise:  $10.03 \text{ m/s}^2$ ). In the 3 branches, the flat profile case achieved the highest helicity density (counterclockwise:  $11.56 \text{ m/s}^2$ , flat profile:  $18.79 \text{ m/s}^2$ , and clockwise:  $7.86 \text{ m/s}^2$ ). Under the counterclockwise case, the swirling flows with the counterclockwise direction are primary in the aorta, while the swirling flows with clockwise direction are primary under both flat case and clockwise case. Moreover, the area of clockwise swirling flow under clockwise case is larger than that under flat profile case. Under both clockwise case and counterclockwise case are larger than that under flat case (counterclockwise:  $5.69 \text{ m/s}^2$ , flat profile:  $3.91 \text{ m/s}^2$ , clockwise:  $5.75 \text{ m/s}^2$ ). Maximum WSS value and the maximum WSSG value generated by clockwise case were lower than in other cases (WSS: counterclockwise 50.48 Pa, Flat profile 25.26 Pa and clockwise 8.80 Pa; WSSG: counterclockwise 33,40 Pa/m, Flat profile 36,84 Pa/m and clockwise 28,53 Pa/m). In brief, the outflow of the BJUT-II VAD has significant effects on the hemodynamics and swirling flow characteristics in the aorta. Compared with the flat profiles, the blood profiles involving a helical component can enhance the strength of aortic swirling flow, and reduce the areas of low WSS and WSSG value regions. Among the 3 cases, the clockwise case may have a benefit for preventing atherosclerosis in the aorta. Moreover, the rotational direction of BJUT-II VAD should be considered as a novel factor that can significantly change the aortic hemodynamic states and swirling flow characteristics.

## References:

1. Mulloy DP, Bhamidipati CM, Stone ML et al: Orthotropic heart transplant versus left ventricular assist device: A national comparison of cost and survival. *J Thorac Cardiovascular Surg*, 2013; 145(2): 566–73
2. Karmonik C, Partovi S, Loebe M et al: Influence of LVAD cannula outflow tract location on hemodynamics in the ascending aorta: A patient-specific computational fluid dynamics approach. *ASAIO J*, 2012; 58(6): 562–67
3. Song ZM, Gu KY, Gao B et al: Hemodynamic effects of various support modes of continuous flow LVADs on the cardiovascular system: A numerical study. *Med Sci Monit*, 2014; (20): 733–41
4. Karmonik C, Partovi S, Schmack B et al: Comparison of hemodynamics in the ascending aorta between pulsatile and continuous flow left ventricular assist devices using computational fluid dynamics based on computed tomography images. *Artif Organs*, 2014; 38(2): 142–48
5. Osorio AF, Osorio R, Ceballos A et al: Computational fluid dynamics analysis of surgical adjustment of left ventricular assist device implantation to minimize stroke risk. *Comput Methods Biomech Biomed Engin*, 2013; 16(6): 622–38
6. Bogren GH, Buonocore HM: 4D magnetic resonance velocity mapping of blood flow patterns in the aorta in young's. Elderly normal subjects. *J Magn Reson Imaging*, 1999; 10(5): 861–69
7. Liu M, Liu X, Kang HY et al: Hemodynamic characteristics of the aorta and its physiological significance. *Journal of Medical Biomechanics*, 2012; 27(5): 481–87
8. Stonebridge PA, Brophy CM: Spiral laminar flow in arteries? *Lancet*, 1991; 338: 1360–61
9. Liu X, Pu F, Fan Y et al: A numerical study on the flow of blood and the transport of LDL in the human aorta: The physiological significance of the helical flow in the aortic arch. *Am J Physiol Heart Circ Physiol*, 2009; 297(1): H163–70
10. Qiu J, Deng X, Fan Y et al: Biomechanical regulation of vascular smooth muscle cell functions: From *in vitro* to *in vivo* understanding. *J R Soc Interface*, 2013; 11(90): 20130852
11. Chang Y, Gao B: Modeling and identification of an ontra-aorta pump. *ASAIO J*, 2010; 56(6): 504–9
12. Gao B, Chang Y, Kaiyun Gu et al: A pulsatile control algorithm of continuous-flow pump for heart recovery. *ASAIO J*, 2012; 58: 343–52
13. Gao B, Nie LY, Chang Y et al: Physiological control of intra-aorta pump based on heart rate. *ASAIO J*, 2011; 57(3): 152–57
14. Chang Y, Gao B, Gu KY: A model-free adaptive control to a blood pump based on heart rate. *ASAIO J*, 2011; 57(4): 262–67
15. Gao B, Gu KY, Zeng Y et al: A blood assist index control by intra-aorta pump: A control strategy for ventricular recovery. *ASAIO J*, 2011; 57(5): 358–62
16. Gao B, Gu KY, Chang Y: An anti-suction control for an intra-aorta pump using blood assistant index. *Artif Organs*, 2012; 36(3): 275–82
17. Gao B, Chang Y, Xuan Y et al: The hemodynamic effect of the support mode for the intra-aorta pump on the cardiovascular system. *Artif Organs*, 2013; 37(2): 157–65
18. Gu K, Gao B, Chang Y et al: The hemodynamic effect of phase differences between the BJUT-II ventricular assist device and native heart on the cardiovascular system. *Artif Organs*, 2014; 38(11): 914–23

19. Qi Z, Bin G, Kaiyun G et al: The study on hemodynamic effect of varied support models of BJUT-II VAD on coronary artery: A primary CFD study. *ASAIO J*, 2014; 60(6): 643–51
20. Xuan Y, Chang Y, Gu K et al: Hemodynamic simulation study of a novel intra-aorta left ventricular assist device. *ASAIO J*, 2012; 58(5): 462–69
21. Fatullayev J, Samak M, Sabashnikov A et al: Continuous-flow left ventricular assist device thrombosis: A danger foreseen is a danger avoided. *Med Sci Monit Basic Res*, 201; 21: 141–44
22. Gu K, Gao B, Chang Y et al: Research on lumped parameter model based on intra-aorta pump. *Journal of Medical Biomechanics*, 2011; 4: 020
23. Hugo GB, Michael HB: Blood flow measurements in the aorta and major arteries with MR velocity mapping. *J Magn Reson Imaging*, 1994; 4: 119–30
24. Gallo D, Steinman DA, Bijari PB et al: Helical flow in carotid bifurcation as surrogate marker of exposure to disturbed shear. *J Biomech*, 2012; 45(2012): 2398–404
25. Liu X, Fan YB, Deng XY: Effect of non-Newtonian and pulsatile blood flow on mass transport in the human aorta. *Journal of Biomechanics*, 2011; 44(6): 1123–31
26. Gallo D, Izu G, Massad D et al: A Survey of quantitative descriptors of arterial flows. visualization and simulation of complex flows in biomedical engineering lecture notes in computational. *Vision and Biomechanics*, 2014; 12: 1–24
27. Shtilmana L, Levichb E, Orszaga SA et al: On the role of helicity in complex fluid flows. *Physics Letters A*, 1985; 113(1): 32–37
28. Ku DN, Giddens DP, Zarins CK, Glagov S: Pulsatile flow and atherosclerosis in the human carotid bifurcation. *Arteriosclerosis*, 1985; 5(3): 293–302
29. Ambardekar AV, Hunter KS, Babu AN et al: Changes in aortic wall structure, composition, and stiffness with continuous-flow left ventricular assist devices: A pilot study. *Circ Heart Fail*, 2015; 8(5): 944–52
30. Templeton DL, John R, Painter P et al: Effects of the left ventricular assist device on the compliance and distensibility of the carotid artery. *Heart Vessels*, 2013; 28(3): 377–84
31. Hasin T, Matsuzawa Y, Guddeti RR et al: Attenuation in peripheral endothelial function after continuous flow left ventricular assist device therapy is associated with cardiovascular adverse events. *Circ J*, 2015; 79(4): 770–77
32. Houston JG, Gandy SJ, Sheppard DG et al: Two-dimensional flow quantitative MRI of aortic arch blood flow patterns: Effect of age, sex, and presence of carotid atheromatous disease on prevalence of spiral blood flow. *J Magn Reson Imaging*, 2003; 18(2): 169–74
33. Yashiro K, Shiratori H, Hamada H: Haemodynamics determined by a genetic programme governs asymmetric development of the aortic arch. *Nature*, 2007; 450(7167): 285–88
34. Javadzadegan A, Fakhim B, Behnia M et al: Fluid-structure interaction investigation of spiral flow in a model of abdominal aortic aneurysm. *Eur J Mech B-Fluid*, 2014; 46: 109–17
35. Chen Z, Fan Y, Deng X et al: Swirling flow can suppress flow disturbances in endovascular stents: A numerical study. *ASAIO J*, 2009; 55(6): 543–49
36. Chiu JJ, Chien S: Effects of disturbed flow on vascular endothelium: Pathophysiological basis and clinical perspectives. *Physiol Rev*, 2011; 91(1): 327–87
37. Gallo D, Steinman DA, Bijari PB et al: Helical flow in carotid bifurcation as surrogate marker of exposure to disturbed shear. *Journal of Biomechanics*, 2012; 45: 2398–404
38. Morbiducci U, Ponzini R, Grigioni M et al: Helical flow as fluid dynamic signature for atherogenesis risk in aortocoronary bypass. A numeric study. *Journal of Biomechanics*, 2007; 40: 519–34
39. Paul MC, Larman A: Investigation of spiral blood flow in a model of arterial stenosis. *Med Eng Phys*, 2009; 31: 1195–203
40. Hyun S, Kleinstreuer C, Archie JP Jr.: Hemodynamics analyses of arterial expansions with implications to thrombosis and restenosis. *Med Eng Phys*, 2000; 22: 13–27
41. Dolan JM, Kolega J, Meng H: High wall shear stress and spatial gradients in vascular pathology: A review. *Ann Biomed Eng*, 2012; 41(7): 1411–27
42. De Bakey ME, Lawrie GM, Glaeser DH: Patterns of atherosclerosis and their surgical significance. *Ann Surg*, 1985; 201: 115–31
43. Caro CG, Fitz GJ, Schroter RC: Arterial wall shear and distribution of early atheroma in man. *Nature*, 1996; 223: 1159–60
44. Malek AM, Alper SL, Izumo S: Hemodynamic shear stress and its role in atherosclerosis. *JAMA*, 1999; 282: 2035–42
45. DePaola N, Gimbrone MA Jr., Davies PF et al: Vascular endothelium responds to fluid shear stress gradients. *Arterioscler Thromb*, 1992; 12(11): 1254–57
46. Lei M, Kleinstreuer C, Truskey GA: Numerical investigation and prediction of atherogenic sites in branching arteries. *J Biomech Eng*, 1995; 117(3): 350–57
47. LaMack JA, Himburg HA, Li XM, Friedman MH: Interaction of wall shear stress magnitude and gradient in the prediction of arterial macro molecular permeability. *Ann Biomed Eng*, 2005; 33(4): 457–64